

Article

Effect of *Phaeodactylum Tricornutum* in Seawater on the Hydration of Blended Cement Pastes

Junjie Wang ¹, Lei Xu ¹, Jiatong Guo ¹, Yimu Jiang ¹, Hang He ², Yuli Wang ^{2,*}, Weiqi Fu ^{3,4,5,†}, Yi Zhu ⁶, Zhe Ye ¹, Pukang He ¹ and Yi Zhang ¹

¹ Department of Civil Engineering, Tsinghua University, Beijing 100084, China

² School of Materials Science and Engineering, Henan Polytechnic University, Jiaozuo 454003, China

³ Department of Marine Science, Ocean College, Zhejiang University, Zhoushan 316021, China

⁴ Donghai Laboratory, Zhoushan 316021, China

⁵ Center for Systems Biology and Faculty of Industrial Engineering, Mechanical Engineering and Computer Science, School of Engineering and Natural Sciences, University of Iceland, 101 Reykjavik, Iceland

⁶ Shenzhen Yichuang International Design Co., Ltd., Shenzhen 518000, China

* Correspondence: wangyuli@hpu.edu.cn

† Senior author.

Abstract: Seawater can be used as mixing water for concrete with no steel reinforcement in some areas with difficult access to fresh water. Diatoms such as *Phaeodactylum tricornutum* are among the most abundant micro-organisms living in seawater, and they could be unavoidable when collecting seawater. In fact, diatoms can provide bio-SiO₂ and bio-CaCO₃ sources, namely amorphous nano-SiO₂ and crystallised nano-CaCO₃, which could be beneficial to cement hydration. Thus, the effects of different *Phaeodactylum tricornutum* concentrations (0%, 2.5% and 5% by weight of suspension of seawater and diatoms) in seawater on cement hydration in ordinary Portland cement (OPC) mixes (100% OPC) and ground granulated blast-furnace slag (GGBS) mixes (70% OPC + 30% GGBS) were investigated through tests of compressive strength, XRD, DTG-DTA and SEM. The results show that diatoms accelerated cement hydration by providing the nucleus for C-S-H structure and contributed pozzolanic reactions by amorphous nano-SiO₂ and nano-CaCO₃. The accelerated cement hydration was also confirmed by the fact that more Ca(OH)₂ was formed in cement pastes with diatoms. However, it has also been found that diatoms decreased the compressive strength of cement pastes by leaving more weak bonds between the C-S-H structure, which was considered to be caused by the organic parts and the micron gap formed in diatoms. When comparing an OPC paste mix with 5% diatoms to a blank OPC paste, the reduction in compressive strength at 28 days can reach a maximum of 50.1%. The ability to provide bridging effects between C-S-H particles in GGBS paste was discovered to depend on the development of additional ettringite. This resulted in a 7.6% loss in compressive strength after 28 days in a GGBS paste with 5% diatoms.

Keywords: diatom; cement hydration; amorphous nano-SiO₂; strength; microstructure



Citation: Wang, J.; Xu, L.; Guo, J.; Jiang, Y.; He, H.; Wang, Y.; Fu, W.; Zhu, Y.; Ye, Z.; He, P.; et al. Effect of *Phaeodactylum Tricornutum* in Seawater on the Hydration of Blended Cement Pastes. *Coatings* **2022**, *12*, 1639. <https://doi.org/10.3390/coatings12111639>

Academic Editor: Andrea Nobili

Received: 10 October 2022

Accepted: 26 October 2022

Published: 28 October 2022

Publisher's Note: MDPI stays neutral with regard to jurisdictional claims in published maps and institutional affiliations.



Copyright: © 2022 by the authors. Licensee MDPI, Basel, Switzerland. This article is an open access article distributed under the terms and conditions of the Creative Commons Attribution (CC BY) license (<https://creativecommons.org/licenses/by/4.0/>).

1. Introduction

In some areas, such as the UAE in the Middle East, with large areas of desert but adjacent to the sea, the use of seawater in plain concrete is unavoidable [1–11]. Recent studies [1,2] have reported that the application of seawater as mixing water in cementitious materials was beneficial for concrete strength development because of the accelerated hydration of cement caused by the salts in seawater [12], and an increase at even above 50% on the compressive strength of ordinary Portland cement (OPC) paste was reported by Wang et al. [1,2]. However, some previous studies showed a reduction in compressive strength when seawater was used as mixing water [12,13]. These conflicts could be caused by the different seawaters used, such as seawater that was filtered through 5 µm by Wang et al. [1,2], but some researchers [12,14] may use unfiltered seawater because filtration steps

take more time and thus increase costs. Impurities such as micro-organisms in seawater could decrease the strength of cementitious materials.

Many micro-organisms, such as diatoms, exist abundantly in seawater and cannot be avoided when pumping water from the sea directly. Locally accumulated diatoms in seawater could exceed 5% by weight of seawater. Thus, the effects of impurities such as micro-organisms on the physical properties of cementitious materials need to be investigated. For simplicity, one of the most abundant micro-organisms in seawater, the diatom, was considered in this study. It is known that diatoms are rich in amorphous nano-SiO₂ [15–20], which could contribute to the hydration of cement. Nano-SiO₂ particles [21–27] could increase the compressive strength of concrete by increasing compactness and providing the nucleus for C-S-H. However, the use of diatoms in seawater also has drawbacks, such as high water demand [28] and a sudden decrease in compressive strength with an increase in dosages [29]. Thus, the substitution quantities of diatoms are generally limited to 10% without compromising strength [28,30]. To the best of the authors' knowledge, no research has ever been conducted on how diatoms affect the hydration of blended cement paste. Thus, the effect of different concentrations of diatoms in seawater (0%, 2.5% and 5% by weight of suspension with seawater and diatoms) on the compressive strength, hydration products and microstructure of OPC and blended cement pastes was investigated. Two types of cement (100% OPC, 70% OPC + 30% GGBS) were considered, to obtain the effect of diatoms in different types of cementitious materials. In this study, the high concentrations of diatoms (2.5% and 5% by weight of seawater and diatoms) were used in order to obtain an obvious effect of the diatoms. Mechanisms of diatoms on cement hydration were analysed through XRD, DTG-DTA and SEM results.

2. Materials and Methods

2.1. Materials

2.1.1. Diatoms

Figure 1a shows the common diatoms contained in seawater (used as mixing water) for the cementitious materials in this study. The name of the diatom is *Phaeodactylum tricornutum* (strain CCAP 1055/1) (CCAP: the culture collection of algae and protozoa). It can be seen that there are two shapes of this diatom, which is because of the different Si contents in their bodies [15,16]. Diatoms were ground into powder using a pestle and mortar. The powder was then passed through a sieve of 75 µm. XRD patterns of diatoms were collected using a Bruker D8 powder diffractometer (Bruker, Karlsruhe, Germany) with scanning angles (2θ) ranging from 5° to 95° at a rate of 0.3 s/step and 0.02°/step using a CuKα radiation source (λ = 1.5418 Å) at 40 kV and 40 mA. Figure 1b shows the XRD patterns of a diatom powder sample, and it can be seen that there are a large number of amorphous nano-SiO₂ particles at about 20–25 degrees and obvious peaks of well-crystallised nano-CaCO₃ and nano-Mg(OH)₂. Figure 1c shows the micromorphology of a raw diatom under SEM, which exhibited a rougher and more irregular structure. The diatom powder was gold-coated and then observed under high-vacuum condition using a JSM7401 field emission scanning electron microscope (JEOL, Eching b., München, Germany).

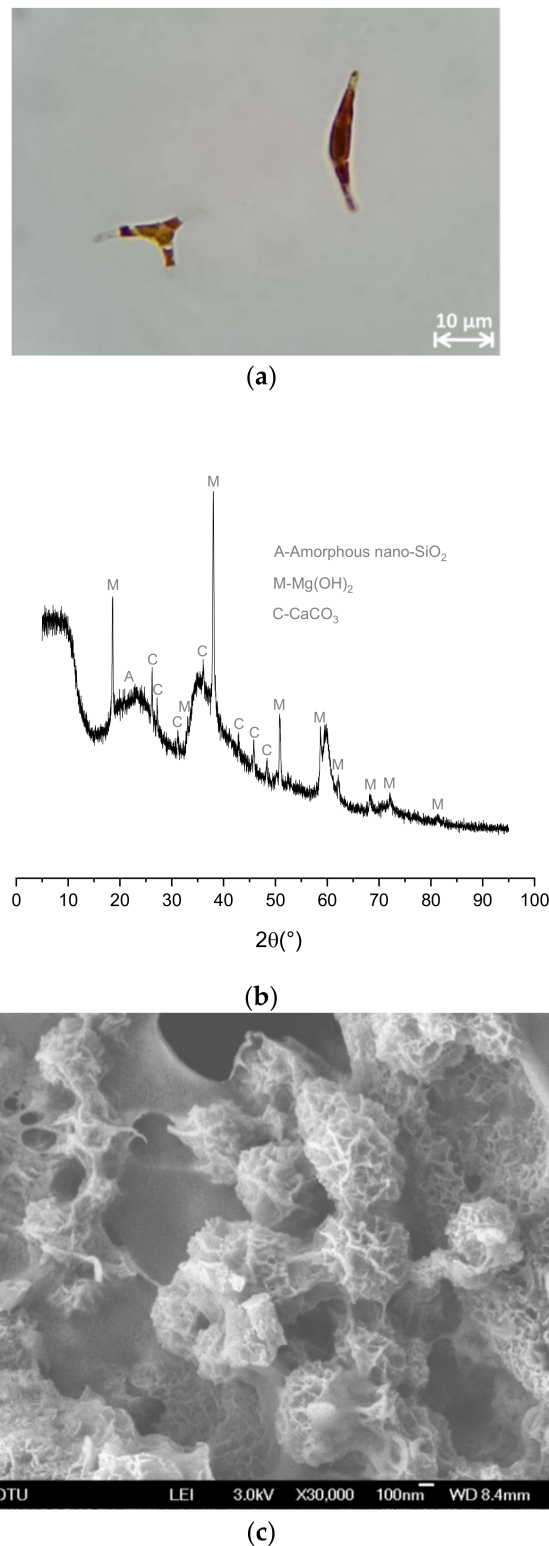


Figure 1. Characterisation of diatoms: (a) Observation of raw diatoms (*P. tricornutum*) under optical microscopy; XRD result (b) and SEM image (c) of diatom powder.

2.1.2. OPC and GGBS

The chemical compositions of OPC (type 1, conforming to ASTM C150M) and GGBS from XRF are shown in Table 1. The results show that GGBS has a much higher content of aluminium phases (Al_2O_3) than OPC and a lower content of CaO.

Table 1. Chemical composition of OPC and GGBS (%).

Composition	CaO	SiO ₂	Al ₂ O ₃	Fe ₂ O ₃	SO ₃	MgO	K ₂ O	Na ₂ O	LOI
OPC	63.02	18.97	5.32	4.26	3.01	1.56	0.54	0.29	3.03
GGBS	34.65	34.33	16.68	1.73	1.79	7.27	0.33	0.25	2.97

2.1.3. Seawater

Seawater from a local beach was collected and used as mixing water for the cementitious materials in this study. Table 2 shows the ion concentration of seawater by ICP-MS [2] after filtration through 5 µm apertures.

Table 2. Ion concentration of seawater.

Ion	Cl ⁻	Na ⁺	Mg ²⁺	SO ₄ ²⁻	K ⁺	Ca ²⁺
Concentration (g/L)	19.67	11.98	2.13	2.06	0.45	0.40

2.2. Mix Proportions and Preparation of Test Samples

The mix design of the samples is shown in Table 3. The effect of diatoms on the hydration of cement paste was considered from three levels of diatoms (0%, 2.5% and 5.0%) and two types of cementitious materials (OPC and GGBS mixes). OPC mixes contained 100% OPC only, and GGBS mixes contained 70% OPC + 30% GGBS. The wt.% of diatoms in seawater is the dry weight of diatoms under 60 °C for 24 h to the weight of the mixed suspension of seawater and diatoms. The different concentrations of diatoms were adjusted by adding different amounts of the filtered seawater.

Table 3. Mix proportions.

Mix ID	w/b	OPC (wt.%)	GGBS (wt.%)	Diatom (wt.%)
OPC	0.4	100	0	0
OPC + 2.5% Diatom	0.4	100	0	2.5
OPC + 5% Diatom	0.4	100	0	5.0
GGBS	0.4	70	30	0
GGBS + 2.5% Diatom	0.4	70	30	2.5
GGBS + 5% Diatom	0.4	70	30	5.0

The mixing procedure was: the OPC powder with or without GGBS was firstly mixed evenly in the mixer, and then, the seawater with different concentrations of diatoms was added with a mixing speed of 133 rpm for 4 min. The fresh pastes were then transferred into 50 mm cube moulds. The moulds with pastes inside were vibrated for 10 s and then transferred into a standard curing chamber (20 °C, R.H. 97%). All samples were demoulded after 24 h and returned to the standard curing chamber until further tests.

2.3. Test Methods

2.3.1. Compressive Strength

After curing for 1, 7 and 28 days in the standard curing chamber, the cubic samples were taken out for compressive strength tests. The tests were conducted in a displacement-controlled mode at a speed of 0.02 mm/s with an MTS machine (MTS Criterion 43, Mechanical Testing & Simulation, Eden Prairie, MN, USA). Three samples were tested for each group.

2.3.2. XRD

The grinding steps of hardened pastes were consistent with those of diatoms. One gram of powder was used for XRD measurement each time. A Rigaku SmartLab XRD machine (Rigaku, Tokyo, Japan) was used. The working voltage was 40 kV, and the current was 150 mA. The scanning was from 5° to 70°, and the scanning rate was 10°/min.

2.3.3. DTG/DTA

The powder samples prepared using the method above were also used for DTG/DTA measurements (HCT-3, Henven Scientific Instrument Factory, Beijing, China). The samples were heated from 25 to 960 °C at a rate of 10 °C/min in a N₂ environment. Samples were stabilised for 20 min in the chamber before the measurements started.

2.3.4. SEM

Selected representative cement paste samples from the inside part of specimens were firstly gold-coated and then observed under high-vacuum condition using a Merlin Compact Field Emission SEM machine (Merlin Compact, Carl Zeiss NTS GmbH, Jena, Germany). The analyses of various morphologies were conducted at 20 kV with a 10 mm working distance.

3. Results and Discussions

3.1. Compressive Strength

Figure 2 shows the results on compressive strength of all mixes after standard curing for 1, 7 and 28 days. It can be seen that the effect of diatoms on cement hydration is different in the different mixes, and it is affected by different concentrations of diatoms in seawater and different cementitious materials. At 1 day, the effect of diatom concentration on the change of compressive strength is not obvious in both OPC and GGBS mixes, and there is only a slight decrease in compressive strength with increasing diatom concentration. However, at 7 and 28 days, the effect of diatom concentration on compressive strength became significant, especially in OPC mixes. In OPC mixes, with the increasing diatom concentrations from 0% to 2.5% and 5%, the decrease in compressive strength was 24.5% and 49.1% at 7 days, and 21.0% and 50.1% at 28 days. In GGBS mixes, with the same increasing diatom concentrations from 0% to 2.5% and 5%, the decrease in compressive strength was 5.2% and 8.6% at 7 days, and only 2.2% and 7.6% at 28 days. It is interesting to see the deleterious effect of diatom on strength development was not as significant in GGBS mixes as in OPC mixes. GGBS mixes can more effectively resist the adverse effects of diatoms on the compressive strength of paste than OPC mixes. From the chemical compositions shown in Table 3, the aluminium phases in GGBS are much higher than in OPC, so the existence of amorphous nano-SiO₂ in the diatoms [17–20] could facilitate additional reaction with the aluminium phases by forming more ettringite in GGBS mixes [31–35] compared to that in OPC mixes, by accelerating the hydration process and providing nucleus sites. The related mechanisms are discussed through the XRD, DTG/DTA and SEM results.

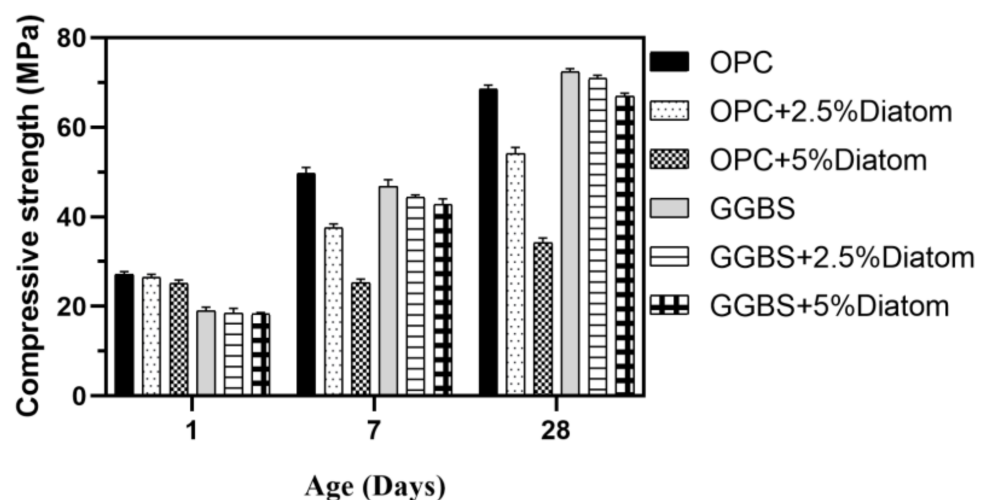
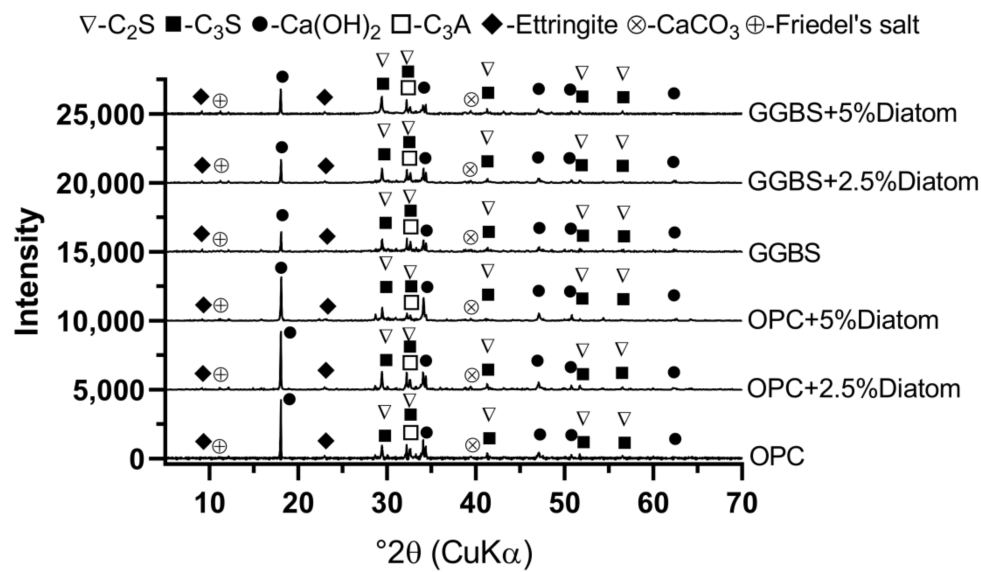


Figure 2. Compressive strength results of different samples at ages of 1, 7 and 28 days.

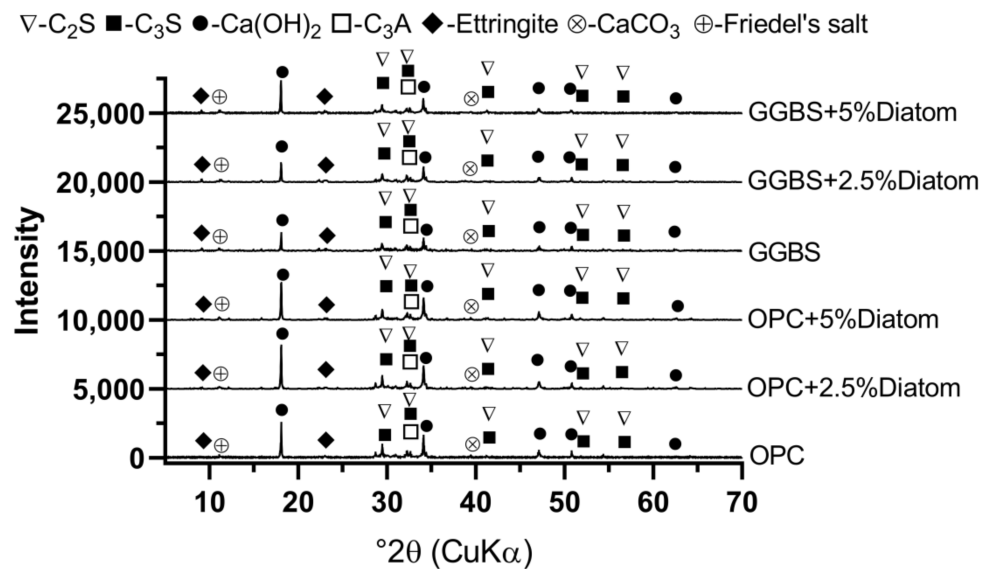
3.2. XRD Results

Figure 3 shows the diffractograms of the crystals identified by XRD in different samples after curing for 1 and 28 days. The relative peak heights can be related to the Y-axis values. It can be seen that the results in OPC mixes and GGBS mixes are different. The peak heights of $\text{Ca}(\text{OH})_2$ in OPC mixes are generally higher than those in GGBS mixes at both 1 and 28 days, which is due to the consumption of $\text{Ca}(\text{OH})_2$ produced by OPC hydration as an alkali activator of GGBS.

It is noted that there are obvious peaks of Friedel's salt in all OPC and GGBS mixes with or without diatoms. The existence of high amounts of chlorides provided the reaction to form Friedel's salt in cement pastes [1,2,7,8]. At 1 day (Figure 3a), the effect of different diatom concentrations on the peak heights and peak areas of $\text{Ca}(\text{OH})_2$ was not obvious. At 28 days (Figure 3b), in both GGBS and OPC mixes, the peak heights and peak areas of $\text{Ca}(\text{OH})_2$ increased gradually with increasing diatom concentrations from 0% to 2.5% and 5%. This could indicate accelerated hydration of C_3S by the existence of amorphous Na-SiO_2 in the diatoms, to some extent. Figure 3 also shows that the peak heights and peak areas of ettringite in GGBS mixes are higher than in OPC mixes, indicating there could be more ettringite in GGBS mixes. This is caused by the higher amounts of aluminium phases in GGBS than OPC, as shown in Table 1.



(a)



(b)

Figure 3. XRD results of different mixes: (a) 1 day, (b) 28 days.

3.3. DTG/DTA Results

Figure 4 shows the effect of different diatom concentrations on the DTG results of the OPC and GGBS mixes after curing for 1 and 28 days. It can be seen that the main peaks correspond to ettringite (80–100 °C [36,37]), Friedel's salt (120, 160 and 360 °C [1,2]), Ca(OH)_2 (450 °C [38,39]) and CaCO_3 (680–720 °C [21,38]), which agrees well with the crystals identified in XRD results (Figure 3). At 1 day, the peaks of ettringite and Ca(OH)_2 in OPC mixes are higher than those in GGBS mixes in Figure 3 because the GGBS has a lower content of CaO and SO_3 than OPC (from Table 1). At 28 days, it is interesting to see that the peak of ettringite in mix OPC + 5% diatom is much lower than that in mix OPC + 2.5% diatom—this could indicate that the amorphous nano- SiO_2 in diatoms may facilitate the transformation of some ettringite to Friedel's salt, which could be evidenced by the higher DTA peak (Figure 5) in the mix OPC + 5% diatom than that in the mix OPC + 2.5% diatom. The fluctuations in Figure 4 at the local range could be caused by the minimal

impurities from the reaction between the trace amounts of other salts (except NaCl) and the OPC minerals or the organic parts in diatoms.

Figure 5 shows the DTA results caused by different diatom concentrations in OPC and GGBS mixes. The corresponding changes in each peak have been marked in the figure, and the differences in each peak can be related to the changes illustrated in Figure 4. The results show that the most obvious energy change occurs at the temperature range of $\text{Ca}(\text{OH})_2$. This agrees well with the DTG results. The difference of DTA results between OPC and GGBS mixes is found to be higher than the difference caused by different diatom concentrations. The DTA peaks of CaCO_3 are not obvious in all mixes, indicating the energy change caused by the decomposition of CaCO_3 in cement pastes is not significant at this stage. Compared to the DTG results, the DTA results could not provide accurate information on the existence of CaCO_3 in cement pastes. Additionally, it was discovered that peaks in the DTA at the sites for ettringite and $\text{Ca}(\text{OH})_2$ could not accurately compare the percentages of these phases.

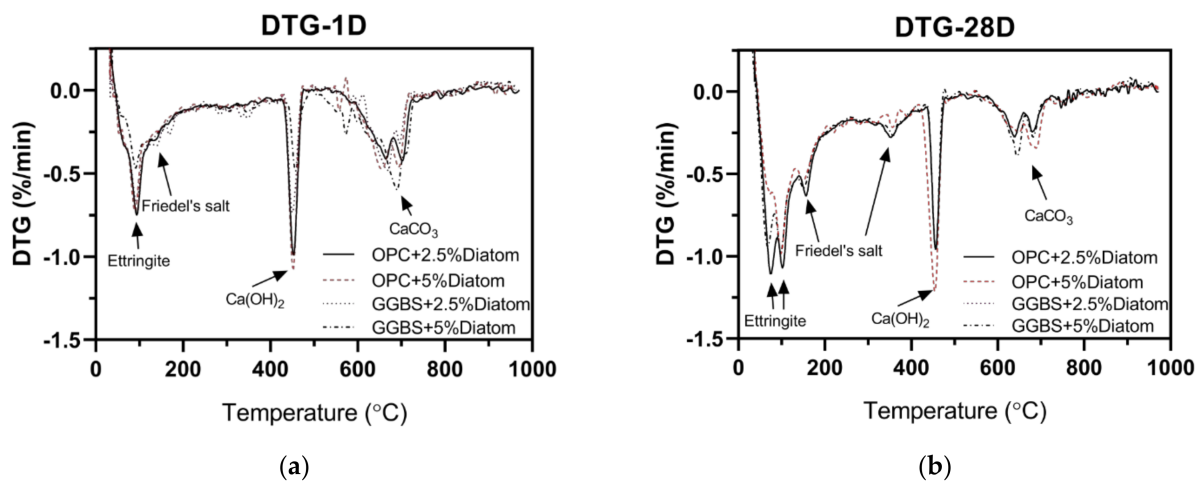


Figure 4. Effect of Diatom on the DTG results of cement paste, (a) 1D, (b) 28 D.

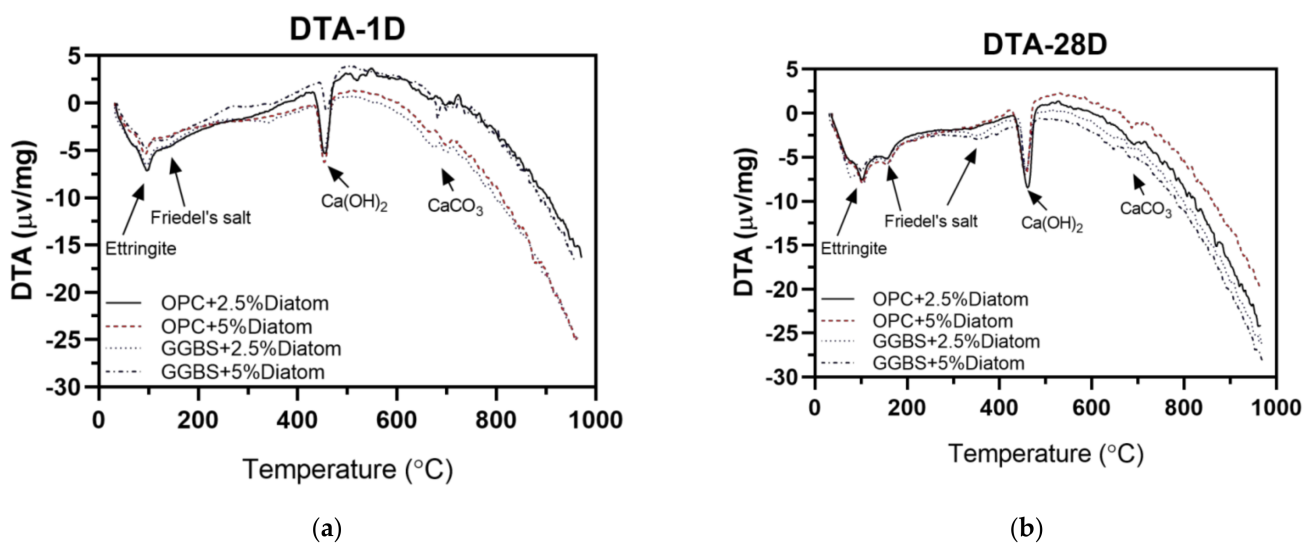


Figure 5. Effect of Diatom on the DTA results of cement paste, (a) 1D, (b) 28 D.

3.4. Microstructure Analysis

Figures 6 and 7 show the microstructure under SEM observations of different OPC and GGBS mixes with 2.5% and 5% diatoms after standard curing for 1 and 28 days. The

existence of ettringite (AFt), $\text{Ca}(\text{OH})_2$ and Friedel's salt can be seen in different mixes. It is found that ettringite is more common than Friedel's salt in the four cement pastes, indicating a higher amount of ettringite was formed than Friedel's salt. This agrees well with the XRD results. It can be clearly seen that, in both OPC and GGBS mixes with 5% diatoms, there are two types of C-S-H [1,40,41], namely low-density C-S-H (LD C-S-H) and high-density C-S-H (HD C-S-H).

By comparing the mixes with 2.5% and 5% diatoms at 1 day in Figure 6, it can be found that, in both OPC and GGBS mixes, the paste with a higher concentration of diatoms (5%) had more clustered nuclear-shaped HD C-S-H. This indicates that the existence of amorphous nano- SiO_2 in diatoms [15–18] and nano- CaCO_3 [37,38] increased the nuclear sites for the formation of the HD C-S-H during the hydration process in cement paste within the early age (1 day). However, the higher amounts of diatoms contain a large amount of amorphous silica, which has high pozzolanic activity and will reduce the compressive strength [42–44] and could also introduce more weak parts in cement pastes. They are mainly caused by two factors, one of which is the organic carbon and moisture present in diatoms, which is evidenced by the disconnection between different piles of clustered nuclear-shaped HD C-S-H in both OPC and GGBS mixes [45–47]. The other is the micron gap formed by the diatoms themselves, which can be obtained by observing the microstructure visually. These agree well with the previously reported results on compressive strength which showed that diatoms in seawater caused a reduction in the compressive strength of cement paste in both OPC and GGBS mixes, especially after 1 day. In GGBS mixes, there is more ettringite formed [48–50], which could provide more bridging effects between disconnected C-S-H particles [51,52] and thus could partly compensate for the strength loss caused by organic parts in diatoms and the micron gap formed by the diatoms. This explains why the GGBS mixes had a lower rate of strength loss with increasing diatom concentration than the OPC mixes, as in Figure 2.

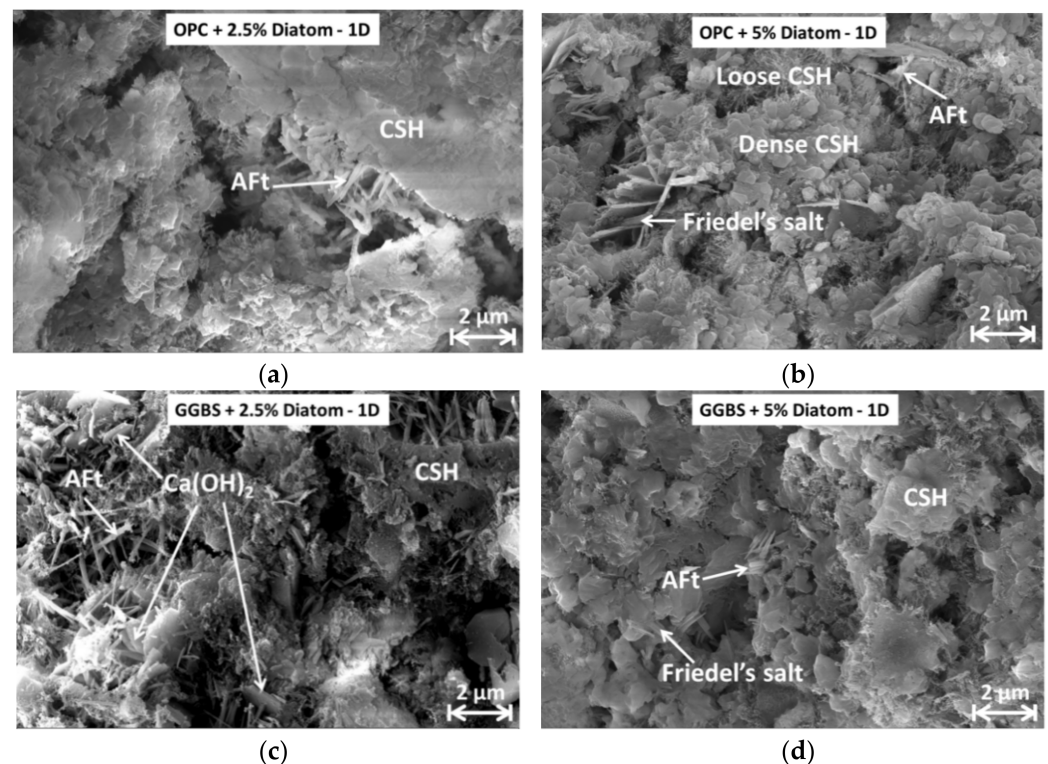


Figure 6. Microstructure observations of different paste samples under SEM at 1D: (a) OPC + 2.5% diatom, (b) OPC + 5% diatom, (c) GGBS + 2.5% diatom, (d) GGBS + 5% diatom.

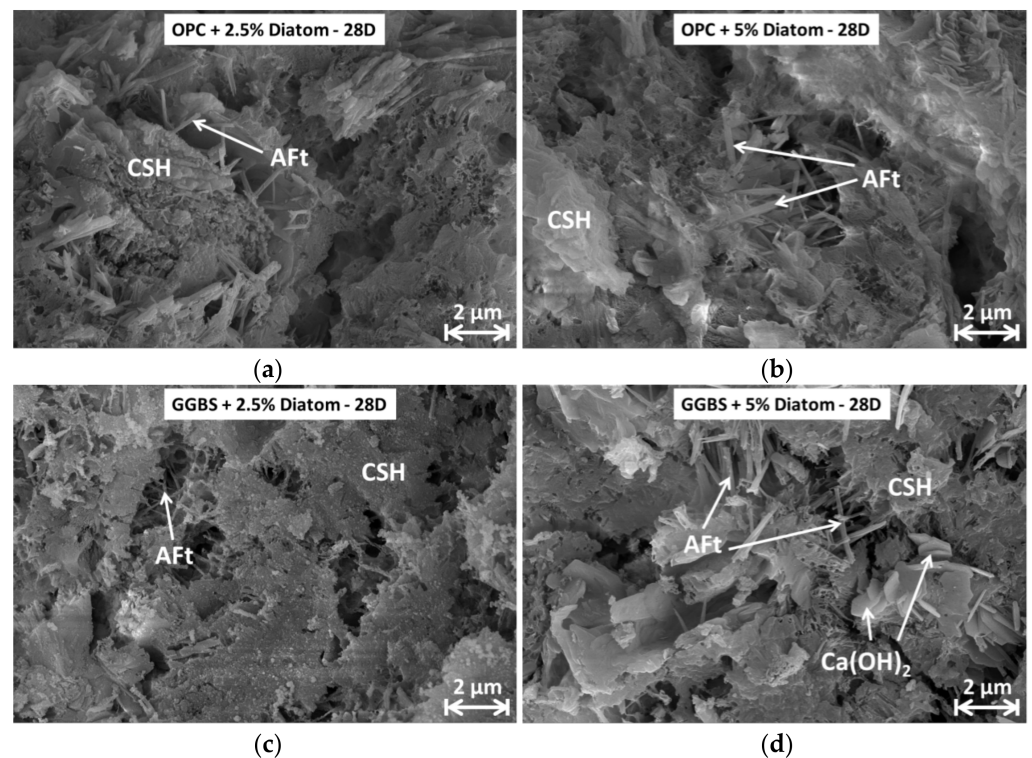


Figure 7. Microstructure observations of different paste samples under SEM at 28D: (a) OPC + 2.5% diatom, (b) OPC + 5% diatom, (c) GGBS + 2.5% diatom, (d) GGBS + 5% diatom.

4. Conclusions

The effect of diatom concentrations (0%, 2.5% and 5% by weight of suspension of seawater and diatoms) on the compressive strength, hydration products and microstructure of OPC and GGBS cement pastes was investigated, and the following conclusions can be drawn:

Diatoms in seawater can accelerate the hydration of cement and produce more Ca(OH)_2 and C-S-H. The microstructure revealed by SEM indicates that the amorphous nano- SiO_2 and nano- CaCO_3 in diatoms could provide the nucleus for C-S-H, and the amorphous nano- SiO_2 also contributes to the pozzolanic reaction in OPC and blended cement paste and thus promotes the hydration of OPC and blended cement.

Although diatoms can accelerate cement hydration, diatoms in seawater are not beneficial for strength development of cement paste, especially after 1 day. This is caused by the organic parts in diatoms and the micron gap formed by the diatoms, which provide weak bonds between C-S-H particles accumulated around the nano- SiO_2 , as evidenced by the SEM results.

The reduction in compressive strength of cement paste with 5% diatoms can be up to 50.1% in OPC mixes, and this reduction is much lower in GGBS mixes, with only up to 8.6%. This difference was thought to be due to the fact that more ettringites formed in GGBS mixes than in OPC mixes, and the ettringites in the early ages provide bridging effects between separated C-S-H particles, thus partly compensating for the detrimental effects of the weak bonds between C-S-H particles in GGBS mixes.

Future research is suggested to investigate the long-term performance of concrete mixed with seawater and diatoms, especially on the GGBS mixes. Further, the allowable maximum concentration of diatoms in seawater should be investigated and quantified. The effect of low-concentrated diatoms in seawater on concrete performance needs to be carried out.

Author Contributions: Conceptualization, J.W., W.F. and Y.Z. (Yi Zhu); methodology, J.W., H.H., Y.W. and W.F.; formal analysis, J.W., L.X., J.G., Y.J., H.H., P.H., Y.Z. and Z.Y. (Yi Zhang); investigation, J.W., L.X., J.G., Y.J., H.H. and Z.Y.; writing—original draft preparation, J.W., L.X. and H.H.; writing—review and editing, J.W., Y.W., W.F., P.H., Y.Z. (Yi Zhang) and Y.Z. (Yi Zhu); supervision, J.W. and Y.W.; project administration, J.W.; funding acquisition, J.W. and Y.W. All authors have read and agreed to the published version of the manuscript.

Funding: The author appreciates the financial support from the National Natural Science Foundation of China (52008232). W.F. was funded by the Hundred Talents Programme of Zhejiang University and also supported by Science Foundation of Donghai Laboratory (Grant No. DH-2022KF0203).

Institutional Review Board Statement: Not applicable.

Informed Consent Statement: Not applicable.

Data Availability Statement: The data presented in this study are available on request from the corresponding author.

Conflicts of Interest: The authors declare no conflict of interest.

References

1. Wang, J.J.; Liu, E.G.; Li, L. Multiscale investigations on hydration mechanisms in seawater OPC paste. *Constr. Build. Mater.* **2018**, *191*, 891–903. [CrossRef]
2. Wang, J.J.; Xie, J.H.; Wang, Y.L.; Liu, Y.L.; Ding, Y.H. Rheological properties, compressive strength, hydration products and microstructure of seawater-mixed cement pastes. *Cem. Concr. Compos.* **2020**, *114*, 103770. [CrossRef]
3. Xiao, J.; Qiang, C.; Nanni, A.; Zhang, K. Use of sea-sand and seawater in concrete construction: Current status and future opportunities. *Constr. Build. Mater.* **2017**, *155*, 1101–1111. [CrossRef]
4. Bazli, M.; Li, Y.L.; Zhao, X.L.; Raman, R.K.S.; Bai, Y.; Al-Saadi, S.; Haque, A. Durability of seawater and sea sand concrete filled filament wound FRP tubes under seawater environments. *Compos. Part B-Eng.* **2020**, *202*, 108409. [CrossRef]
5. Dhondy, T.; Remennikov, A.; Sheikh, M.N. Properties and Application of Sea Sand in Sea Sand-Seawater Concrete. *J. Mater. Civ. Eng.* **2020**, *32*, 04020392. [CrossRef]
6. Yang, J.L.; Lu, S.W.; Wang, J.Z.; Wang, Z. Behavior of CFRP partially wrapped square seawater sea-sand concrete columns under axial compression. *Eng. Struct.* **2020**, *222*, 111119. [CrossRef]
7. Dasar, A.; Patah, D.; Hamada, H.; Sagawa, Y.; Yamamoto, D. Applicability of seawater as a mixing and curing agent in 4-year-old concrete. *Constr. Build. Mater.* **2020**, *259*, 119692. [CrossRef]
8. Mangi, S.A.; Makhija, A.; Raza, M.S.; Khahro, S.H.; Jhatal, A.A. A Comprehensive Review on Effects of Seawater on Engineering Properties of Concrete. *Silicon* **2021**, *13*, 4519–4526. [CrossRef]
9. Zhang, Y.R.; Wei, Y.; Bai, J.W.; Wu, G.; Dong, Z.Q. A novel seawater and sea sand concrete filled FRP-carbon steel composite tube column: Concept and behaviour. *Compos. Struct.* **2020**, *246*, 112421. [CrossRef]
10. Li, Y.L.; Zhao, X.L.; Raman, R.K.S. Durability of seawater and sea sand concrete and seawater and sea sand concrete-filled fibre-reinforced polymer/stainless steel tubular stub columns. *Adv. Struct. Eng.* **2020**, *24*, 1074–1089. [CrossRef]
11. Chen, G.M.; Liu, P.C.; Jiang, T.; He, Z.B.; Wang, X.M.; Lam, L.; Chen, J.F. Effects of natural seawater and sea sand on the compressive behaviour of unconfined and carbon fibre-reinforced polymer-confined concrete. *Adv. Struct. Eng.* **2020**, *23*, 3102–3116. [CrossRef]
12. Mbadike, E.M.; Elinwa, A.U. Effect of salt water in the production of concrete. *Niger. J. Technol.* **2011**, *30*, 105–110. Available online: <https://nijotech.com/index.php/nijotech/article/view/31> (accessed on 1 October 2022).
13. Younis, A.; Ebead, U.; Suraneni, P.; Nanni, A. Fresh and hardened properties of seawater-mixed concrete. *Constr. Build. Mater.* **2018**, *190*, 276–286. [CrossRef]
14. Montanari, L.; Suraneni, P.; Tsui-Chang, M.; Khatibmasjedi, M.; Ebead, U.; Weiss, J.; Nanni, A. Hydration, Pore Solution, and Porosity of Cementitious Pastes Made with Seawater. *J. Mater. Civ. Eng.* **2019**, *31*, 04019154. [CrossRef]
15. De Martino, A.; Bartual, A.; Willis, A.; Meichenin, A.; Villazan, B.; Maheswari, U.; Bowler, C. Physiological and Molecular Evidence that Environmental Changes Elicit Morphological Interconversion in the Model Diatom *Phaeodactylum tricorutum*. *Protist* **2011**, *162*, 462–481. [CrossRef] [PubMed]
16. Tesson, B.; Gaillard, C.; Martin-Jezequel, V. Insights into the polymorphism of the diatom *Phaeodactylum tricorutum* Bohlin. *Bot. Mar.* **2009**, *52*, 104–116. [CrossRef]
17. Moreno, J.J.G.; Pan, K.; Wang, Y.; Li, W.J. Computational Study of APTES Surface Functionalization of Diatom-like Amorphous SiO₂ Surfaces for Heavy Metal Adsorption. *Langmuir* **2020**, *36*, 5680–5689. [CrossRef]
18. Yilmaz, E.U.; Yilmaz, M. Diatom-Derived SiO₂/N-Doped C Nanocomposite for Electrochemical Capacitors. *ECS J. Solid State Sci. Technol.* **2020**, *9*, 061012. [CrossRef]
19. Zhang, D.Y.; Pan, J.F.; Cai, J.; Wang, Y.; Jiang, Y.G.; Jiang, X.G. Hydrofluoric acid-assisted bonding of diatoms with SiO₂-based substrates for microsystem application. *J. Micromech. Microeng.* **2012**, *22*, 035021. [CrossRef]

20. Dudley, S.; Kalem, T.; Akinc, M. Conversion of SiO₂ diatom frustules to BaTiO₃ and SrTiO₃. *J. Am. Ceram. Soc.* **2006**, *89*, 2434–2439. [[CrossRef](#)]
21. Wang, Y.L.; Lu, H.J.; Wang, J.J.; He, H. Effects of Highly Crystallized Nano C-S-H Particles on Performances of Portland Cement Paste and Its Mechanism. *Crystals* **2020**, *10*, 816. [[CrossRef](#)]
22. Long, G.; Li, Y.; Ma, C.; Xie, Y.; Shi, Y. Hydration kinetics of cement incorporating different nanoparticles at elevated temperatures. *Thermochim. Acta* **2018**, *664*, 108–117. [[CrossRef](#)]
23. Nuaklong, P.; Sata, V.; Wongsas, A.; Srinavin, K.; Chindaprasirt, P. Recycled aggregate high calcium fly ash geopolymer concrete with inclusion of OPC and nano-SiO₂. *Constr. Build. Mater.* **2018**, *174*, 244–252. [[CrossRef](#)]
24. Shaikh, F.U.; Supit, S.W.; Salim, B. Microstructure and Nanoscaled Characterization of HVFA Cement Paste Containing Nano-SiO₂ and Nano-CaCO₃. *J. Mater. Civ. Eng.* **2017**, *29*, 04017063. [[CrossRef](#)]
25. Mohseni, E.; Miyandehi, B.M.; Yang, J.; Yazdi, M.A. Single and combined effects of nano-SiO₂, nano-Al₂O₃ and nano-TiO₂ on the mechanical, rheological and durability properties of self-compacting mortar containing fly ash. *Constr. Build. Mater.* **2015**, *84*, 331–340. [[CrossRef](#)]
26. Xu, L.; Wang, J.; Li, K.; Lin, S.; Li, M.; Hao, T.; Ling, Z.; Xiang, D.; Wang, T. A systematic review of factors affecting properties of thermal-activated recycled cement, Resources. *Conserv. Recycl.* **2022**, *185*, 106432. [[CrossRef](#)]
27. Pourjavadi, A.; Fakoorpoor, S.M.; Khaloo, A.; Hosseini, P. Improving the performance of cement-based composites containing superabsorbent polymers by utilization of nano-SiO₂ particles. *Mater. Des.* **2012**, *42*, 94–101. [[CrossRef](#)]
28. Li, J.; Zhang, W.; Li, C.; Monteiro, P.J.M. Green concrete containing diatomaceous earth and limestone: Workability, mechanical properties, and life-cycle assessment. *J. Clean. Prod.* **2019**, *223*, 662–679. [[CrossRef](#)]
29. Aydin, A.C.; Gül, R. Influence of volcanic originated natural materials as additives on the setting time and some mechanical properties of concrete. *Constr. Build. Mater.* **2007**, *21*, 1277–1281. [[CrossRef](#)]
30. Degirmenci, N.; Yilmaz, A. Use of diatomite as partial replacement for Portland cement in cement mortars. *Constr. Build. Mater.* **2009**, *23*, 284–288. [[CrossRef](#)]
31. Wang, J.; Xu, L.; Li, M.; He, H.; Wang, Y.; Xiang, D.; Lin, S.; Zhong, Y.; Zhao, H. Effect of pre-carbonation on the properties of cement paste subjected to high temperatures. *J. Build. Eng.* **2022**, *51*, 104337. [[CrossRef](#)]
32. Wang, J.J.; Xie, J.H.; Wang, C.H.; Zhao, J.B.; Liu, F.; Fang, C. Study on the optimum initial curing condition for fly ash and GGBS based geopolymer recycled aggregate concrete. *Constr. Build. Mater.* **2020**, *247*, 118540. [[CrossRef](#)]
33. Xie, J.H.; Liu, J.F.; Liu, F.; Wang, J.J.; Huang, P.Y. Investigation of a new lightweight green concrete containing sludge ceramics and recycled fine aggregates. *J. Clean. Prod.* **2019**, *235*, 1240–1254. [[CrossRef](#)]
34. Wang, J.; Basheer, P.A.M.; Nanukuttan, S.V.; Long, A.E.; Bai, Y. Influence of service loading and the resulting micro-cracks on chloride resistance of concrete. *Constr. Build. Mater.* **2016**, *108*, 56–66. [[CrossRef](#)]
35. Alhozaimy, A.; Al-Negheimish, A.; Alawad, O.A.; Jaafar, M.S.; Noorzaeei, J. Binary and ternary effects of ground dune sand and blast furnace slag on the compressive strength of mortar. *Cem. Concr. Compos.* **2012**, *34*, 734–738. [[CrossRef](#)]
36. He, Z.; Zhu, X.; Wang, J.; Mu, M.; Wang, Y. Comparison of CO₂ emissions from OPC and recycled cement production. *Constr. Build. Mater.* **2019**, *211*, 965–973. [[CrossRef](#)]
37. Wang, J.; Liu, E.; Li, L. Characterization on the recycling of waste seashells with Portland cement towards sustainable cementitious materials. *J. Clean. Prod.* **2019**, *220*, 235–252. [[CrossRef](#)]
38. Wang, J.J.; Liu, E.G. Upcycling waste seashells with cement: Rheology and early-age properties of Portland cement paste. *Resour. Conserv. Recycl.* **2020**, *155*, 104680. [[CrossRef](#)]
39. Wang, Y.; He, F.; Wang, J.; Hu, Q. Comparison of Effects of Sodium Bicarbonate and Sodium Carbonate on the Hydration and Properties of Portland Cement Paste. *Materials* **2019**, *12*, 1033. [[CrossRef](#)]
40. Constantinides, G.; Ulm, F.J. The effect of two types of C-S-H on the elasticity of cement-based materials: Results from nanoindentation and micromechanical modeling. *Cem. Concr. Res.* **2004**, *34*, 67–80. [[CrossRef](#)]
41. Constantinides, G.; Ulm, F.J.; Van Vliet, K. On the use of nanoindentation for cementitious materials. *Mater. Struct.* **2003**, *36*, 191–196. [[CrossRef](#)]
42. Liu, J.; Wu, K.W.; Wang, Y.F.; Yang, Y.Q. Effects of fly Ash/diatomite admixture with variable particle sizes on the mechanical properties and porosity of concrete. *J. Wuhan Univ. Technol. -Mater. Sci. Ed.* **2017**, *32*, 1072–1079. [[CrossRef](#)]
43. Yilmaz, B. A study on the effects of diatomite blend in natural pozzolan-blended cements. *Adv. Cem. Res.* **2008**, *20*, 13–21. [[CrossRef](#)]
44. Senff, L.; Hotza, D.; Labrincha, J.A. Effect of diatomite addition on fresh and hardened properties of mortars investigated through mixture experiments. *Adv. Appl. Ceram.* **2011**, *110*, 142–150. [[CrossRef](#)]
45. Xie, J.; Zhao, J.; Wang, J.; Fang, C.; Yuan, B.; Wu, Y. Impact behaviour of fly ash and slag-based geopolymeric concrete: The effects of recycled aggregate content, water-binder ratio and curing age. *Constr. Build. Mater.* **2022**, *331*, 127359. [[CrossRef](#)]
46. Hang, H.; Wang, Y.; Wang, J. Effects of aggregate micro fines (AMF), aluminum sulfate and polypropylene fiber (PPF) on properties of machine-made sand concrete. *Appl. Sci.* **2019**, *9*, 2250.
47. Wang, J.; Xie, J.; He, J.; Sun, M.; Zhao, J. Combined use of silica fume and steel fibre to improve fracture properties of recycled aggregate concrete exposed to elevated temperature. *J. Mater. Cycles Waste Manag.* **2020**, *22*, 862–877. [[CrossRef](#)]
48. Wang, J. Steady-state chloride diffusion coefficient and chloride migration coefficient of cracks in concrete. *J. Mater. Civ. Eng.* **2017**, *29*, 0417117. [[CrossRef](#)]

49. Wang, J.; Liu, E. The relationship between steady-state chloride diffusion and migration coefficients in cementitious materials. *Mag. Concr. Res.* **2020**, *72*, 1016–1026. [[CrossRef](#)]
50. Xie, J.; Zhao, J.; Wang, J.; Huang, P.; Liu, J. Investigation of the high-temperature resistance of sludge ceramsite concrete with recycled fine aggregates and GGBS and its application in hollow blocks. *J. Build. Eng.* **2021**, *34*, 101954. [[CrossRef](#)]
51. Li, J.Q.; Jin, Q.X.; Zhang, W.X.; Li, C.; Monteiro, P.J.M. Microstructure and durability performance of sustainable cementitious composites containing high-volume regenerative biosilica. *Resour. Conserv. Recycl.* **2022**, *178*, 106038. [[CrossRef](#)]
52. Liu, R.Q.; Yang, Y.Q.; Zhao, X.K.; Pang, B. Quantitative phase analysis and microstructural characterization of Portland cement blends with diatomite waste using the Rietveld method. *J. Mater. Sci.* **2021**, *56*, 1242–1254. [[CrossRef](#)]